A FREQUENCY-SELECTING TECHNIQUE FOR MOBILE HANDSET ANTENNAS BASED ON CAPACITANCE SWITCHING

Cheol Yoon[1, *], Sun-Gook Hwang[1], Gi-Chan Lee[1], Woo-Su Kim[2], Hwa-Choon Lee[3], Cheon-Hee Lee[4], and Hyo-Dal Park[1]

[1]Department of Electronics Engineering, Inha University, YongHyun-dong Nam-gu Incheon, Republic of Korea

[2]Information and Communication Engineering, KEIT, Yeoksam-dong Gangnam-gu, Seoul, Republic of Korea

[3]Department of Information and Communications Engineering, Chodang University, Muan-gun Cheon-nam, Republic of Korea

[4]System Integration Team/R&D Center Ace Technologies Corp., Nonhyeon-dong Incheon, Republic of Korea

Abstract—This paper introduces a mobile switchable antenna for long term evolution (LTE) of the 4th generation (4G), applicable to all mobile service bands. The validity of this antenna is assessed by design, realization, and measurement. A new frequency-selecting method is used in the proposed antenna, based on capacitance switching among four states. Due to the limited antenna space in existing terminals, it is quite difficult to cover the entire low band with a single antenna. To overcome this difficulty, three single-pole double-throw (SPDT) switches, one 74HC04, and four capacitors are used. The resulting antenna covers the LTE (698–798 MHz) and GSM (824–960 MHz) bands in the low-band characteristic by realizing four capacitance states and at the same time covers the DCS (1710–1880 MHz)/PCS (1850–1990 MHz)/WCDMA (1920–2170 MHz) bands in the high-band characteristic. The antenna provides a gain of −1.04–6.00 dBi, a radiation efficiency of 32.73–74.99%, and omnidirectional characteristics in the H-plane. Because of this outstanding performance, it is expected that the new frequency - selecting technique will be applied in 4G mobile communication terminals.

1. INTRODUCTION

Recently, market structure and corporate activities around the world have been changing swiftly in response to rapid growth in the information and communication markets. Most of the mobile communication companies are expected to develop their services from the global system for mobile communications (GSM) and code division multiple access (CDMA) into long term evolution (LTE). The LTE market is currently being energized, and mobile communication services and devices are expected to include various networks and services. Therefore, the antennas used in these devices are required to support not only 2nd generation (2G) and wideband code division multiple access (WCDMA) bandwidth, but also LTEs, and research on that subject is needed [1–7].

Antennas for mobile phones must be small and must operate in multi-bands. A planar inverted-F antenna (PIFA) structure is widely used to provide these characteristics. However, this structure has a narrow bandwidth and low efficiency in bands lower than 800 MHz. Thus, it is difficult to cover a wide bandwidth with a single PIFA [8–13]. To overcome this difficulty, research has been carried out on antennas that can vary their operating frequency electrically [14–17].

It is possible to attain size reduction with similar radiation characteristics and gain, as well as wider effective bandwidth, by making an antenna reconfigurable, because it operates in multiple frequency ranges using a single radiator. Furthermore, interference from adjacent frequencies can be minimized with a frequency-selecting capability. Hence, a reconfigurable antenna offers many advantages because it can simultaneously optimize input impedance, radiation characteristics, and polarization characteristics without transforming the physical structure of the radiator. According to current trends, RF-MEMS switches [18], PIN diodes [19], and varactor diodes [20] are typically used to tune the operating frequencies of existing reconfigurable antennas.

In this paper, a new frequency-selecting technique is introduced to resolve these issues, using three single-pole double-throw (SPDT) switches, one 74HC04 (NOT gate), and four chip capacitors. The proposed switchable antenna offers many advantages; first, it operates on less than 3.7 V which is the typical operating voltage of mobile phone batteries. Second, it has high frequency selectivity because the state varies among four states by DIP switches. Moreover, covered frequency range at low-band by switching is about 272 MHz (32.81%), and the capacitances can be chosen to different values when the shape of the antenna has to be changed or different bands are needed. The high-

band (DCS/PCS/WCDMA) characteristic is attained with PIFA and the low-band (LTE/GSM) characteristic by switching the states of a DIP switch. The values of the capacitors are $C_1 = 2.0 \, \text{pF}$, $C_2 = 1.5 \, \text{pF}$, $C_3 = 1.0 \, \text{pF}$, $C_4 = 0.5 \, \text{pF}$, and these are determined from simulation results. CST Microwave Studio is used as a simulation tool to design the antenna and analyze its performance, and the optimum antenna that attains the characteristic of each band is realized. A prototype antenna was fabricated to assess the validity of the structure, and its performance was evaluated via measurement.

2. PRINCIPLE OF THE SWITCHING OPERATION AND ANTENNA DESIGN

2.1. Controlling the Operational Characteristics of the Antenna by Varying the Capacitance

Figure 1 shows the typical structure of PIFAs. The resonant frequency of a PIFA is defined by its width W, length L, speed of the light c, and effective dielectric constant ε_{eff} and is given by (1).

$$f = \frac{c}{4\sqrt{\varepsilon_{eff}}\,(W + L)} \tag{1}$$

The resonant frequency of an antenna is determined by its input impedance. The input impedance of a PIFA can be decomposed into resistance and reactance components, as in (2).

$$Z_{in} = R_{in} + jX_{in} \tag{2}$$

In this study, a capacitor is added between the end of the PIFA and the ground in order to obtain the desired characteristics. The structure and equivalent circuit of this antenna are shown in Figures 2(a)
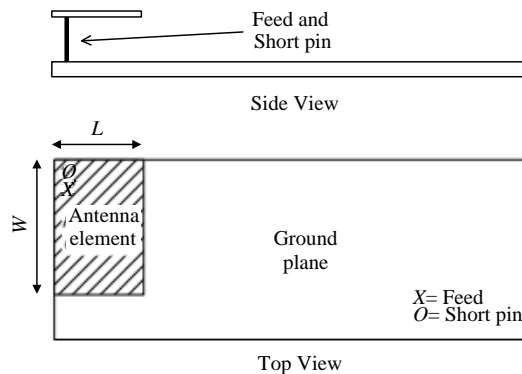

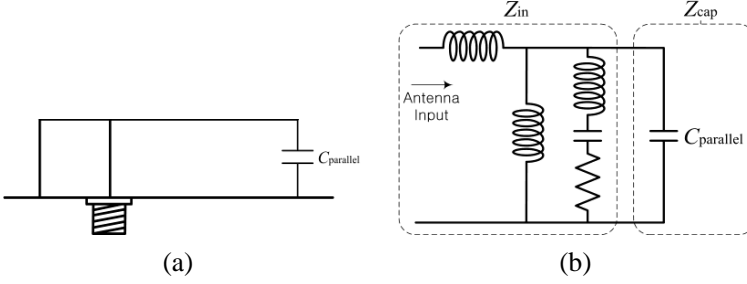**Figure 1.** Typical structure of the PIFAs.

Figure 2. Proposed inverted-F antenna: (a) geometry, (b) equivalent circuit.

and (b). To obtain the resonant frequency, the impedance of the parallel capacitor is applied to (2). The result is expressed as (3).

$$f = \frac{X}{2\pi C \left(X^2 + R^2\right)} \tag{3}$$

Equation (3) implies that the resonant frequency decreases as C increases, and resonance at a lower frequency means that the electrical length of the antenna increases. Therefore, the length L of the PIFA becomes $L + \Delta L$ when the capacitor is attached in parallel. Accordingly, (1) is modified to (4).

$$f = \frac{c}{4\sqrt{\varepsilon_{eff}} \left(W + (L + \Delta L)\right)} \tag{4}$$

2.2. Principle of the Switching Operation

Based on the theoretical discussion of Section 2.1, four capacitance states are realized, using three SPDTs and one 74HC04 (NOT gate). Figure 3(a) shows the logic symbol and the application circuit for the SPDT switch component. The battery voltage is controlled between ON and OFF by the DIP switch, and the voltage signal is reversed in 74HC04. Pin 5 of the SPDT chooses between RF1 and RF2 via contrary input signals to pins 4 and 6. The paths of the signals are listed in Table 1 according to the control input.

Figure 3(b) shows the logic symbol of the KSD-42H DIP switch, whose structure includes four switches toggling between the ON and OFF states. Pin 1 is connected to VDD and pins 2–4 to the input of the 74HC04 component.

Because the SPDT switch operates properly through NOT gates, the 74HC04 component (which is composed of six NOT gates) is connected to the input of the SPDT. Figure 3(c) shows the logic
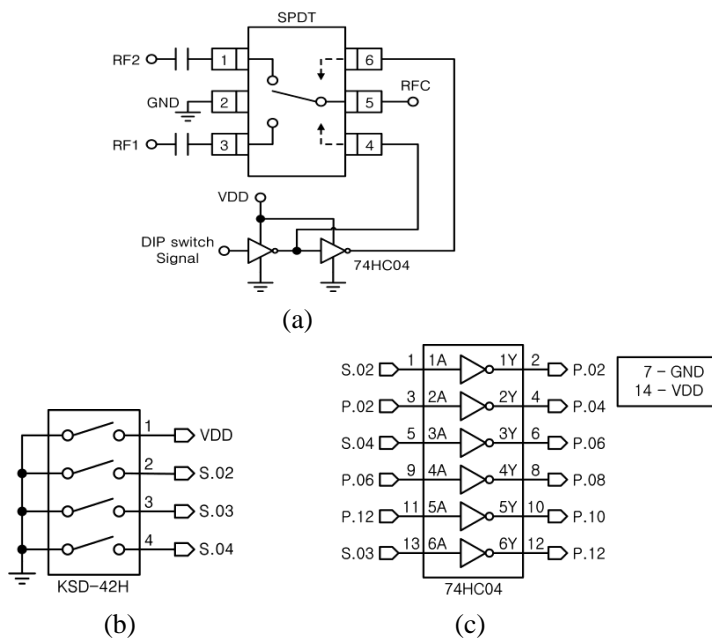
Figure 3. Logic diagram of the device: (a) SPDT switch application circuit, (b) DIP switch, (c) 74HC04 logic symbol.

Table 1. Signal path according to SPDT input.

Control input		Signal path	
4	6	RF1	RF2
High	Low	ON	OFF
Low	High	OFF	ON

symbol of the 74HC04. As the figure indicates, input signals from the DIP switch are inverted by the internal NOT gates of the 74HC04. The inverted signal is then inverted one more time and connected to another input of the SPDT. As a result, signals from the DIP switch are divided into two contrary signals and become the input signals of the SPDT.

A logic diagram of the proposed antenna is shown in Figure 4. Three SPDTs are connected together, and their control inputs are connected to the DIP switch. The signals from the DIP switch control the states of the SPDTs, causing one of the capacitors to be selected.
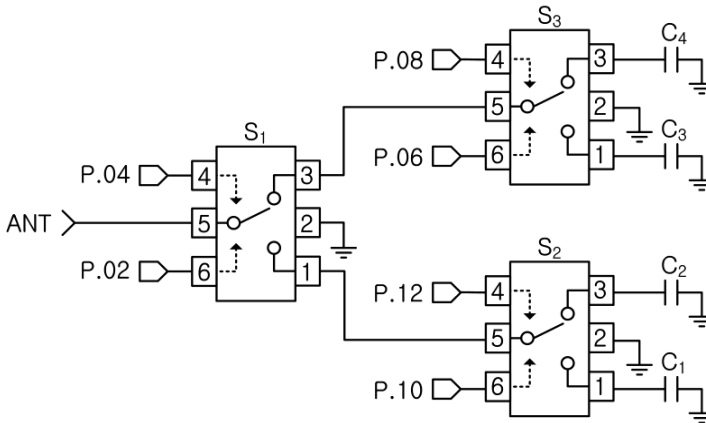
Figure 4. Logic diagram of the switchable antenna.

Table 2. Capacitance state table.

Capacitance state	DIP switch control				Value
	1	2	3	4	
State 1	ON	OFF	ON	-	C_1 (2.0 pF)
State 2	ON	OFF	OFF	-	C_2 (1.5 pF)
State 3	ON	ON	-	OFF	C_3 (1.0 pF)
State 4	ON	ON	-	ON	C_4 (0.5 pF)

(-): Conditions that are not considered.

The chosen capacitor is connected to the antenna, and the operating frequency is determined by the capacitances. Starting at S_1, the inverted output of P.02 is inverted one more time. Therefore, signals from P.02 and P.04 have opposite values, and S_1 is connected to S_2 or S_3. When S_1 is connected to S_2, C_1 or C_2 is selected by the signals from P.10 and P.12. If S_1 is connected to S_3, C_3 or C_4 is selected by the signals from P.06 and P.08. In all cases, the chosen capacitor is connected to the antenna. The capacitances are listed in Table 2 according to the input from the DIP switch.

Prior to concluding this section, insertion losses by using switches need to be considered since it can change the total characteristic of the antenna compared to the ideal case. Since there are two SPDTs on the signal route to the capacitor, power level of the signals are reduced by two SPDTs. The loss by the SPDT used in this paper is 0.25–0.40 dB at 1–2 GHz according to the manufacturer. Therefore, the total loss by switches will be about 0.5–0.8 dB.

2.3. Antenna Design

Figure 5 shows the structure of the antenna and switches described in Section 2.2. The dimensions, which include the antenna and ground plane in a mobile phone application, are $W = 60\,\text{mm}$, $L_1 = 107\,\text{mm}$, and $L_2 = 13\,\text{mm}$. This is the typical size of a bar-type smartphone.

Figure 5(a) shows a 3D view of the overall configuration of the circuit, and it can be seen that the end of the radiator is connected to the SPDT. Figure 5(b) shows the unfolded structure of the radiator. The PIFA was designed based on the Equation (1) introduced in Section 2.1. According to the equation, resonance frequency is affected by width and length of the PIFA. Therefore, the radiator for low frequency should be longer (dotted line), and the radiator for high frequency be shorter (solid line).

Figure 6 shows a zoomed image of the configuration of part A in Figure 5(a), which is the key component of the switching operation.
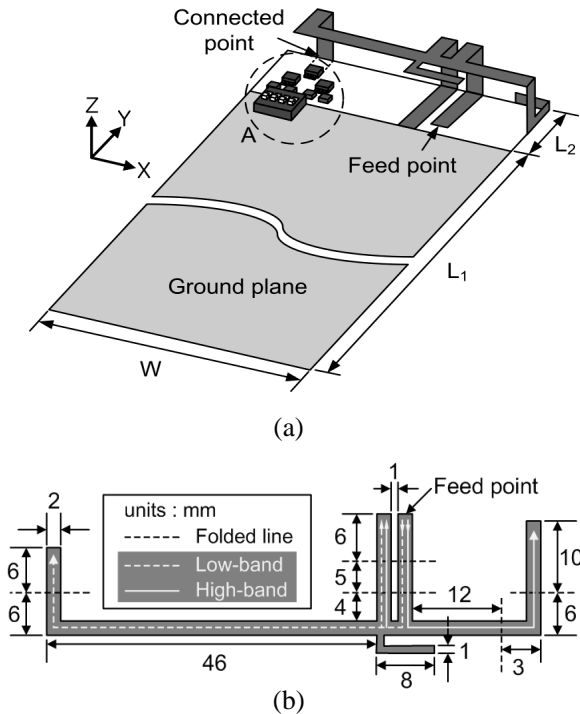

(a)

(b)

Figure 5. Configuration of the antenna design: (a) 3D view, (b) dimensions and contributions to each band.
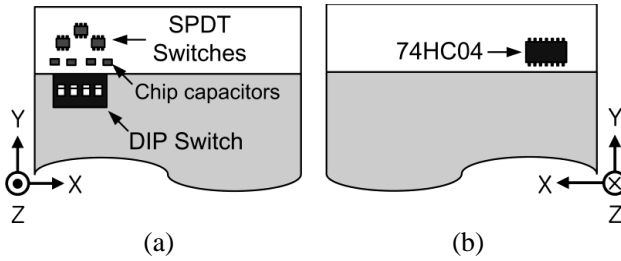
Figure 6. Zoomed image of the configuration of A in Figure 4(a):
(a) top, (b) bottom.

Figure 6(a) shows the top side of the PCB, to which the DIP switch,
four capacitors (C_1, C_2, C_3, C_4 from left to right), and three SPDT
switches are attached. Figure 6(b) shows the bottom side of the PCB,
to which the 74HC04 is attached.

3. SIMULATION AND MEASUREMENT

Design and optimization of the antenna were implemented with the
simulation software CST Microwave Studio. Based on the LTE, GSM,
DCS, PCS, and WCDMA standards, the antenna was designed to
operate with linear polarization and VSWR lower than $3 : 1$ (-6 dB)
at operating frequencies [21–23].
     Figure 7 shows the simulation results for the VSWR character-
istics. To attain switchable antenna characteristics, capacitors were
attached at the end of the radiator, which resonated in the low band.
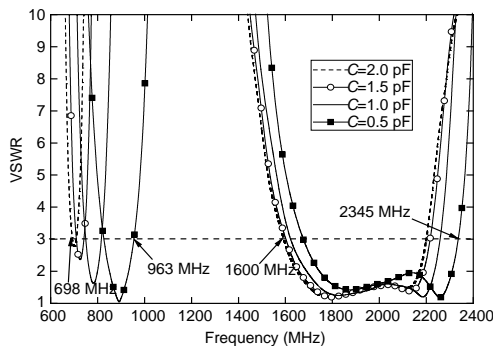In the simulation, the resonant frequency of the antenna was shifted

Figure 7. Simulated VSWR characteristics of the antenna.

by varying the capacitance.

The selected capacitances were 0.5 pF, 1.0 pF, 1.5 pF, and 2.0 pF. When the capacitance was 2.0 pF, the antenna resonated at 698 MHz (LTE band), and by gradually decreasing the capacitance to 0.5 pF, the antenna was made to satisfy the GSM band characteristic. Although the high band characteristic indicated that the resonant frequency was slightly shifted depending on the capacitance, all bands from DCS to WCDMA were covered.

A prototype antenna was fabricated and simulated using the optimized parameters determined by the operational principle and simulation explained in Section 2. The PCB was fabricated on a substrate with a relative dielectric constant ε_r of 4.4 and a thickness of 1 mm. The configuration of the measurement environment is shown in Figure 8. Figure 8(a) shows the entire configuration, and Figures 8(b) and (c) show the layout of the switching part. The sizes of the fabricated radiator and ground were $50 \times 13 \times 3.2$ mm and $60 \times 107 \times 1$ mm, respectively, and the total size of the PCB was
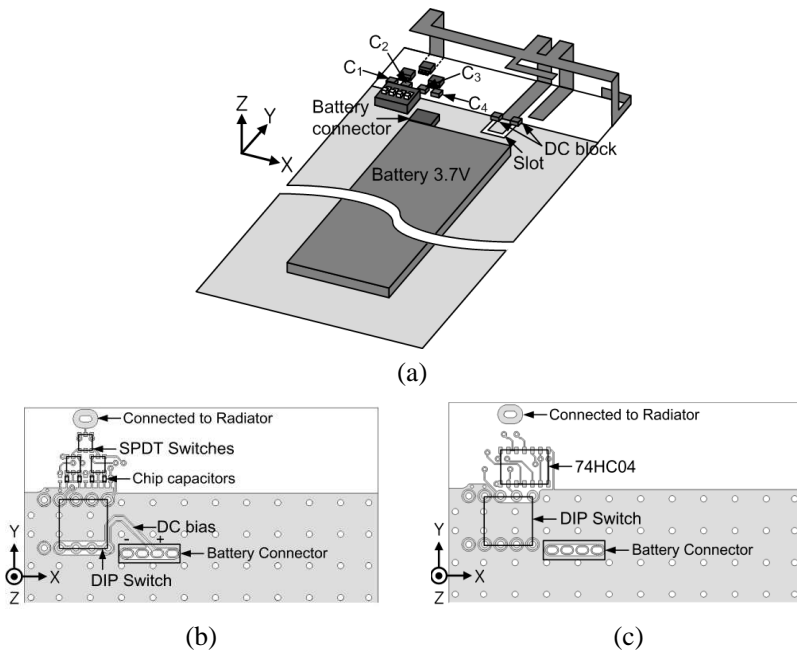

(a)

(b)

(c)

Figure 8. Configuration of measurement environment: (a) the entire configuration, (b) top shape of the layout, (c) bottom shape of the layout.

$60 \times 120 \times 3.2$ mm, which is the typical size of smartphones currently on the market. When 3.7 V (the usual battery voltage) is biased to the DIP switch, depending on the DIP switch status, the voltage is biased to the 74HC04 and SPDT devices, and positive voltage then flows to the ground along the radiator pattern. To avoid this shorting problem, a slot is used to create a voltage potential between the ground and the radiator. A DC block of 56 pF compensates for the performance change of the antenna caused by the slot and blocks the flow of direct current to the ground.

The VSWR characteristics of the fabricated antenna were measured using an Agilent Technologies E5071C Network Analyzer with a coaxial cable, and the radiation patterns were measured in an anechoic chamber.

Figure 9 shows the measured VSWR characteristics of the fabricated antenna. The measurements were carried out in the 600–2400 MHz range, and for VSWR lower than 3 : 1 (-6 dB), the resonant
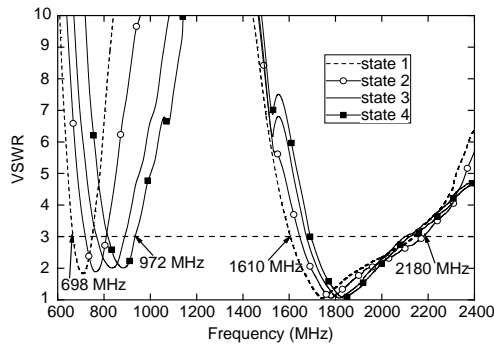

**Figure 9.** Measured VSWR characteristics of the fabricated antenna.

Table 3. Radiation efficiency and gain.

| State	Operation Frequency [MHz]	Radiation Efficiency [%]	Gain [dBi]
State 1	698–770	32.73–50.82	−1.04–1.84
	1710–2170	42.66–63.53	2.80–5.45
State 2	752–836	40.64–59.57	0.79–2.42
	1710–2170	45.29–63.92	3.08–5.59
State 3	791–918	41.50–69.18	0.76–2.90
	1710–2170	46.88–64.57	3.15–5.60
State 4	834–972	40.18–62.09	0.41–2.37
	1710–2170	52.97–74.99	2.81–6.00

frequency shifted from 698–972 MHz as the state changed from state 1 to state 4. These results are similar to the predicted characteristics, and the fabricated antenna covered all service bands, including the LTE and GSM bands.

Figure 10 shows the radiation patterns of the four states, measured from 0° to 360° at intervals of 5°. In all of the states, the antenna exhibited an omnidirectional radiation pattern characteristic in the H-plane.

Figure 11 shows the measured gain of the antenna in each state, and the values of radiation efficiency and gain are arranged in Table 3. In Figure 11, it is found that the gain at low-band is low compared to the gain of high-band. It is assumed that the reason of the low gain is because of the losses at switches and capacitors. However, this value is not considered as a defect because it shows an excellent performance compared to currently manufactured antenna. Overall, it is expected that the proposed antenna will provide effective signal reception, because it shows outstanding gain and radiation patterns over all bands and has an omnidirectional radiation pattern in the H-plane, regardless of the direction of transmission.
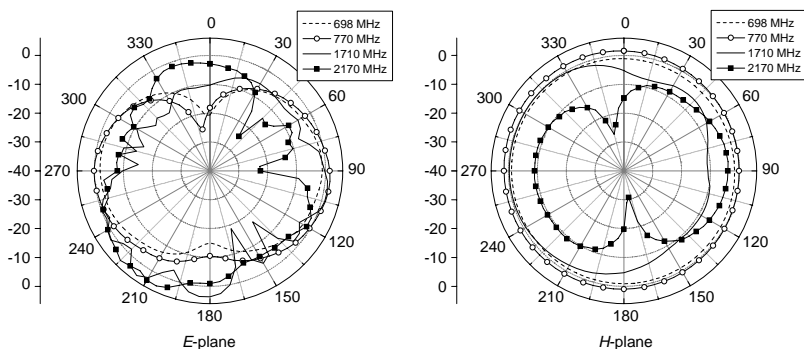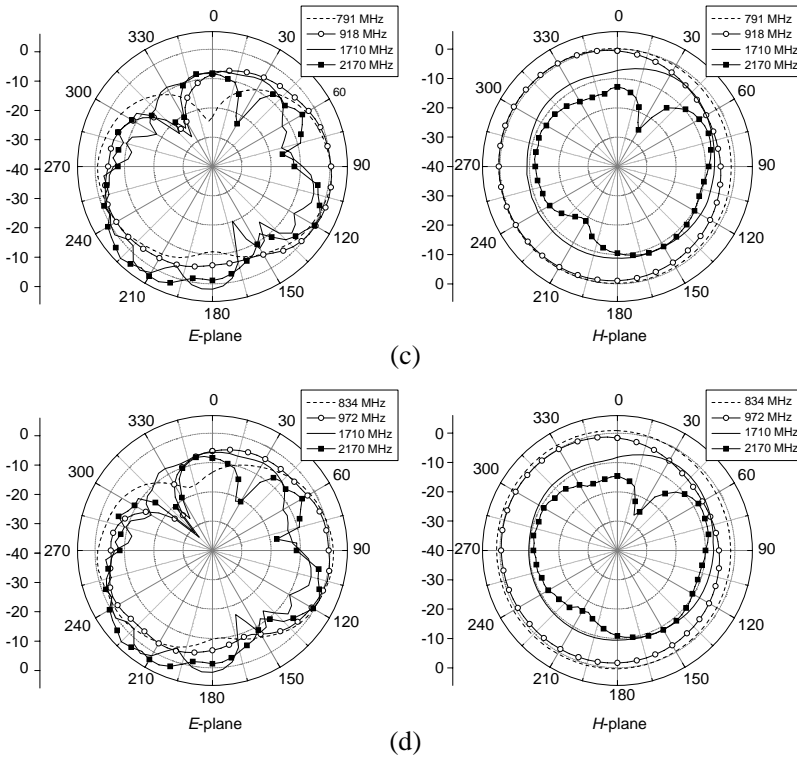

(a)
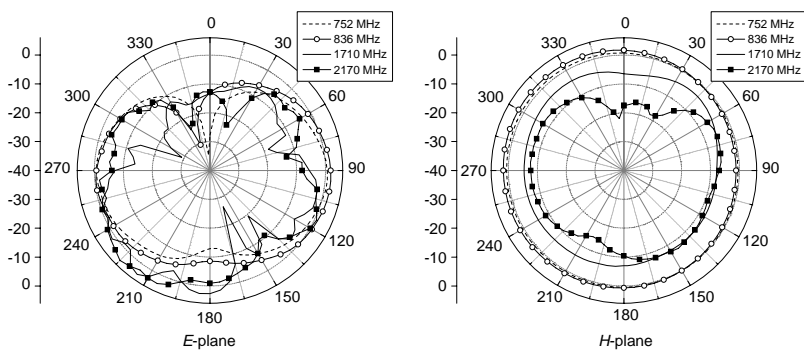
(b)

Figure 10. Measured radiation patterns: (a) state 1, (b) state 2, (c) state 3, (d) state 4.
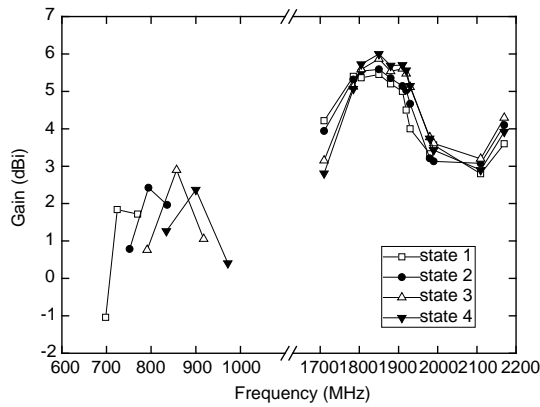

Figure 11. Gain of the antenna measured in each state.

4. CONCLUSIONS

A frequency-selecting technique for mobile terminal antennas was researched, which can be applied to LTE, as well as other mobile communication service bands.

Starting with a basic PIFA structure to attain a high-band (DCS/PCS/WCDMA) characteristic, a low-band (LTE/GSM) characteristic of 698–960 MHz was attained by selecting one of four capacitances, using one DIP switch, three SPDT switches, and one 74HC04 (NOT gate). The four capacitances are 0.5 pF, 1.0 pF, 1.5 pF, and 2.0 pF. The measurement results were as follows. As the capacitance state changed from state 1 to state 4, the operating frequency of the low band shifted from 698–972 MHz, while satisfying the typical VSWR standard below 3 : 1 (−6 dB). The proposed antenna exhibited a gain of −1.04–6.00 dBi in all bands, a radiation efficiency of 32.73–74.99%, and omnidirectional characteristics in the H-plane. Its overall performance was remarkable, exceeding the standards in all bands.

In LTE, two antennas must be installed because a multi-input/multi-output (MIMO) system is applied as a standard. Hence, the isolation between the antennas and the envelope correlation coefficient (ECC) must be considered. If an antenna is added to the switchable antenna, and the required isolation and ECC characteristics are satisfied, the proposed antenna is expected to provide an excellent structure for a MIMO antenna for LTE.

ACKNOWLEDGMENT

REFERENCES

1. Kim, W.-S., C. Yoon, S.-S. Oh, S.-Y. Kang, and H.-D. Park, "Broadband planar antenna with T-shaped strip and capacitively coupled shorted strip," *Microwave and Optical Technology Letters*, Vol. 53, No. 9, 1980–1983, 2011.

2. Sesia, S., M. Baker, and I. Toufik, *LTE — The UMTS Long Term Evolution: From Theory to Practice,* 1–6, Wiley, 2009.

3. Thomas, H. J., D. L. Fudge, and G. Morris, "Gunn source integrated with a micro-strip patch," *Microwaves and RF*, Vol. 24, No. 2, 87–89, 1985.

4. Chang, K., K. A. Hummer, and G. Gopalakrishna, "Active radiating element using FET source integrated with micro-strip patch antenna," *Electronics Letters*, Vol. 24, No. 21, 1347–1348, 1988.

5. Haskings, P. M., P. S. Hall, and J. S. Dahele, "Active patch antenna element with diode tuning," *Electronics Letters*, Vol. 27, No. 20, 1846–1847, 1991.

6. Liao, P. and R. A. York, "A varactor-tuned patch oscillator for active arrays," *IEEE Microwave and Guided Wave Letters*, Vol. 4, No. 10, 335–337, 1994.

7. Navarro, J. A., Y. Shu, and K. Chang, "Broadband electronically tunable planar active radiating elements and spatial power combiners using notch antennas," *IEEE Trans. Microwave Theory Tech.*, Vol. 40, No. 2, 323–328, 1992.

8. Yoon, C., W.-K. Park, S.-Y. Kang, and H.-D. Park, "A spiral-shaped monopole antenna for quad-band operation of mobile handsets," *Microwave and Optical Technology Letters*, Vol. 50, No. 11, 2860–2863, 2008.

9. Lee, W.-J., C. Yoon, S.-U. Kim, and H.-D. Park, "A study on isolation enhancement of MIMO antenna using differential ground path," *Microwave and Optical Technology Letters*, Vol. 54, No. 3, 802–805, 2012.

10. Cho, J., C. W. Jung, and K. Kim, "Frequency-reconfigurable two-port antenna for mobile phone operating over multiple service bands," *Electronics Letters*, Vol. 45, 1009–1011, 2009.

11. Hsiao, F. R., H. T. Chen, G. Y. Lee, T. W. Chiou, and K. L. Wong, "A dual-band planar inverted-F patch antenna with a branch-line slit," *Microwave and Optical Technology Letters*, Vol. 32, 310–312, 2002.

12. Rowell, C. R. and R. D. Murch, "A compact PIFA suitable for dual frequency 900/1800-MHz operation," *IEEE Transactions on Antennas and Propagation*, Vol. 46, 596–598, 1998.

13. Wong, K. L., W. C. Su, and F. S. Chang, "Wideband internal folded planar monopole antenna for UMTS/WiMAX folder-type mobile phone," *Microwave and Optical Technology Letters*, Vol. 48, 324–327, 2006.

14. Waterhouse, R. B. and N. Y. Shuley, "Frequency agile microstrip rectangular patches using varactor diodes," *URSI Radio Science Meeting and Nuclear EMP Meeting*, Vol. 4, 2188–2191, 1992.

15. Fan, L. and K. Chang, "An active inverted patch antenna with wideband varactor-tuned capability," *IEEE MTT-S International*

Microwave Sumposium Digest, Vol. 2, 923–926, 1996.

16. Zhang, J. and A. Mortazawi, "An L-band tunable microstrip antenna using multiple varactors," *Antennas and Propagation Society International Symposium*, Vol. 4, 524–527, 2003.

17. Carrasquillo-Rivera, I., Z. Popovic, and R. A. R. Solis, "Tunable slot antenna using varactors and photodiodes," *Antennas and Propagation Society International Symposium*, Vol. 4, 532–535, 2003.

18. Besoli, A. G. and F. De Flaviis, "A multifunctional reconfigurable pixeled antenna using MEMS technology on printed circuit board," *IEEE Transactions on Antennas and Propagation*, Vol. 59, No. 12, 4413–4424, 2011.

19. Li, Y., Z. Zhang, W. Chen, Z. Feng, and M. F. Iskander, "A switchable matching circuit for compact wideband antenna designs," *IEEE Transactions on Antennas and Propagation*, Vol. 58, No. 11, 3450–3457, 2010.

20. Lim, J.-H., G.-T. Back, Y.-I. Ko, C.-W. Song, and T.-Y. Yun, "A reconfigurable PIFA using a switchable PIN-diode and a fine-tuning varactor for USPCS/WCDMA/m-WiMAX/WLAN," *IEEE Transactions on Antennas and Propagation*, Vol. 58, No. 7, 2404–2411, 2010.

21. Ban, Y.-L., J.-H. Chen, S.-C. Sun, J. L.-W. Li, and J.-H. Guo, "Printed wideband antenna with chip-capacitor-loaded inductive strip for LTE/GSM/UMTS WWAN wireless USB dongle applications," *Progress In Electromagnetics Research*, Vol. 128, 313–329, 2012.

22. Chen, Z., Y.-L. Ban, J.-H. Chen, J. L.-W. Li, and Y.-J. Wu, "Bandwidth enhancement of LTE/WWAN printed mobile phone antenna using slotted ground structure," *Progress In Electromagnetics Research*, Vol. 129, 469–483, 2012.

23. Kang, W., K. H. Ko, and K. Kim, "A compact beam reconfigurable antenna for symmetric beam switching," *Progress In Electromagnetics Research*, Vol. 129, 1–16, 2012.